J|A|C|S
ARTICLES
Published on Web 03/15/2006

Intramolecular Electron Transfer through the 20-Position of a Chlorophyll *a* Derivative: An Unexpectedly Efficient Conduit for Charge Transport

Richard F. Kelley, Michael J. Tauber, and Michael R. Wasielewski*

Contribution from the Department of Chemistry and International Institute of Nanotechnology, Northwestern University, Evanston, Illinois 60208-3113

Received December 4, 2005; E-mail: m-wasielewski@northwestern.edu

Abstract: Suzuki cross-coupling reactions have afforded 20-phenyl-substituted Chlorophyll *a* derivatives (ZCPh) in good yields and significant quantities from readily available Chl *a*. A series of donor−acceptor dyads was synthesized in which naphthalene-1,8:4,5-bis(dicarboximide) or either of two perylene-3,4:9,-10-bis(dicarboximide) electron acceptors is attached to the para position of the 20-phenyl group. Comparisons with the analogous dyads based on a zinc 5,10,15-tri(*n*-pentyl)-20-phenylporphyrin donor show that, for a given acceptor and solvent, the rates of photoinduced charge separation and recombination as well as the calculated electronic coupling matrix elements, *V*, for these reactions differ by less than a factor of 2. However, EPR and ENDOR spectroscopy corroborated by DFT calculations show that the highest occupied MO of $ZCPh^{+\bullet}$ has little spin (charge) density at the 20-carbon atom, whereas $Z3PnPh^{+\bullet}$ has significant spin (charge) density there, implying that *V*, and therefore the electron-transfer rates, should differ significantly for these two macrocyclic donors. DFT calculations on $ZCPh^{+\bullet}$ and $Z3PnPh^{+\bullet}$, with two −0.5 charges located where the nearest carbonyl oxygen atoms of the acceptor would reside in the donor−acceptor dyads, show that the presence of the negative charges significantly shifts the charge density of both $ZCPh^{+\bullet}$ and $Z3PnPh^{+\bullet}$ from the macrocycle onto the phenyl rings. Thus, the presence of adjacent covalently linked radical anions at a fixed location relative to each of these radical cations results in nearly identical electronic coupling matrix elements for electron transfer and therefore very similar rates.

Introduction

Photosynthetic antenna and reaction center proteins serve as important models for developing synthetic light-harvesting and photochemical charge separation systems.[1,2] Chlorophylls have strong electronic absorptions in both the blue and red regions of the visible spectrum, thus providing excellent solar spectral coverage. The intense lowest energy Q_y electronic transition in chlorophylls is strongly polarized along the ring A−ring C axis, and the coupling of this transition dipole to those of other chlorophylls is largely responsible for many of the spectral forms that are observed for chlorophylls in proteins. The spatial relationships between chlorophylls bound to proteins are maintained using weak interactions, such as ligation of their central magnesium atoms to histidines and hydrogen bonding of their oxygen-containing functional groups to nearby amino acids. Notable exceptions to this binding motif are the chlorophylls present in the peripheral antenna system of green sulfur bacteria, which engage in direct chlorophyll−chlorophyll association to produce large cylindrical arrays of pigments.[3−6]

Chlorophyll *a* (Chl *a*) and its derivatives self-assemble in vitro into large aggregates using two principal structural motifs.[7,8] First, in the absence of other nucleophiles, the 13^1-ketone of one Chl *a* serves as an axial ligand for the Mg of another Chl *a*. Second, the presence of a hydrogen-bonding nucleophile, such as water or an alcohol, ROH, results in ligation of the Mg of one Chl *a* by the oxygen atom of ROH, while the H atom of ROH hydrogen-bonds to the 13^1-ketone of another Chl *a*. Both motifs result in *J*-type aggregates having red-shifted optical transitions.[9] In most biomimetic Chl-based systems synthesized previously, electron acceptors have been attached to positions on the Chl macrocycle that limit the ability of the system to self-assemble into supramolecular structures by either changing the steric requirements for assembly or introducing additional intermolecular interactions. For example, the 3b-vinyl position of Chl *a* has been functionalized with bulky triptycene-quinone,[10] arylene bis(dicarboximide),[11,12] and C_{60}[13−15] electron acceptors. The shapes and sizes of these acceptors prevent the often desirable self-association of the Chl *a* derivatives along

(1) Wasielewski, M. R. *Chem. Rev.* **1992**, *92*, 435−461.
(2) Gust, D.; Moore, T. A.; Moore, A. L. *Acc. Chem. Res.* **1993**, *26*, 198−205.
(3) Staehelin, L. A.; Golecki, J. R.; Drews, G. *Biochim. Biophys. Acta* **1980**, *589*, 30−45.
(4) Worcester, D. L.; Michalski, T. J.; Tyson, R. L.; Bowman, M. K.; Katz, J. J. *Physica B (Amsterdam, Neth.)* **1989**, *156−157*, 502−504.
(5) Blankenship, R. E.; Olson, J. M.; Miller, M. In *Anoxygenic Photosynthetic Bacteria*; Blankenship, R. E., Madigan, M. T., Bauer, C. E., Eds.; Kluwer: Dordrecht, 1995; pp 399−435.
(6) van Rossum, B. J.; Steensgaard, D. B.; Mulder, F. M.; Boender, G. J.; Schaffner, K.; Holzwarth, A. R.; de Groot, H. J. M. *Biochemistry* **2001**, *40*, 1587−1595.
(7) Katz, J. J. *Inorganic Biochemistry*; Elsevier: Amsterdam, 1973; Vol. 2.
(8) Katz, J. J.; Shipman, L. L.; Cotton, T. M.; Janson, T. R. *Porphyrins* **1978**, *5*, 401−458.
(9) Kasha, M.; Rawls, H. R. *Pure Appl. Chem.* **1965**, *11*, 371−392.

the ring A−ring C axis. Holzwarth et al.[13] compared the self-assembly characteristics of pyro-Chl *a* having a C_{60} rigidly linked to its 3-position to those of the corresponding molecule having a C_{60} flexibly attached at the less sterically hindered 17^3-position. They concluded that the self-assembly characteristics of the pyro-Chl *a* should only be preserved by attaching C_{60} to the 17^3-position. The ability to attach electron acceptors to the Chl macrocycle in a rigid fashion without interfering with functional groups that are essential to self-assembly is important for developing photofunctional structures that carry out rapid, directional energy and charge transport.[1,2,16−20]

The 20-position of Chl *a* offers a potential site for rigid attachment of either redox or energy-transfer components that should not interfere with self-assembly. Using the 20-position of Chl *a* as a conduit for charge transport is unprecedented, although several related synthetic chlorin-acceptor molecules have been previously studied. Lindsey has prepared a series of synthetic oxochlorin dyads in which zinc and magnesium oxochlorins are linked to the corresponding free bases using phenyl and phenylethynyl linkers.[21−23] Laser flash photolysis studies of these molecules show that energy transfer from the metallo-oxochlorins to the free base is slower than that observed for the corresponding porphyrin systems. This difference is attributed to through-bond Dexter-type energy transfer, which depends critically on the electron density distribution in the frontier molecular orbitals of the donor and acceptor,[21] as well as the properties of the linker group.[22] Kirmaier et al.[23] have studied electron transfer from similar metallo-oxochlorins to a perylene-3,4:9,10-bis(dicarboximide) (PDI) molecule linked to the 10-position of the oxochlorin using a diphenylacetylene spacer. Photoexcitation of PDI in these dyads results in competitive singlet−singlet energy transfer to the oxochlorin and electron transfer from the oxochlorin to ^{1}*PDI. Electron transfer from the photoexcited oxochlorin to PDI is relatively slow, even in polar solvents, due primarily to free energy considerations. Direct comparisons of the electron-transfer characteristics of the oxochlorin dyads with the corresponding porphyrin dyads were not reported.

It is well known that the rates of both Dexter-type energy transfer and electron transfer to or from metalloporphyrins depend on the position of the macrocycle to which the donor or acceptor is attached.[24−28] The rates of these transfers, k_{DA}, are given by $k_{DA} \propto V_{DA}^2$(FCWD), where V_{DA} is the electronic coupling matrix element and FCWD is the Franck−Condon weighted density of states (see below).[29−31] Since the matrix element V_{DA} depends on orbital overlap between the frontier molecular orbitals of the metalloporphyrin and those of the donor or acceptor,[32] rates of Dexter-type energy transfer and electron transfer depend on the electron density distributions within these orbitals.[24,33] The two highest occupied molecular orbitals (HOMO and HOMO−1) within metalloporphyrins are nearly degenerate and have electron density distributions that differ greatly.[34−36] The a_{1u} orbital has significant electron density at the β carbons of the porphyrin with little density at the meso positions, while the opposite is true for the a_{2u} orbital. The energetic ordering of these two orbitals in the metalloporphyrin depends on the nature and the position of the substituents attached to the porphyrin.[36] Substituting electron-donating groups, e.g., phenyl rings or alkyl chains, at the meso positions (5,10,15,20) of the porphyrin raises the energy of the a_{2u} orbital above that of the a_{1u} orbital, making the a_{2u} orbital the HOMO. On the other hand, substitution of the β positions with similar electron-releasing groups results in the a_{1u} orbital being the HOMO. This is consistent with EPR data obtained for zinc *meso*-tetraphenylporphyrin radical cation, which shows that its meso positions have significantly greater spin (and charge) density compared to those at the β positions.[36] It is also consistent with EPR measurements on related zinc porphyrins having a mix of both alkyl and aryl substituents at their meso positions,[37] which all show that the a_{2u} orbital is the zinc porphyrin HOMO. Generally, increased electron density at particular peripheral carbon atoms of the porphyrin results in stronger electronic coupling to molecules attached to those positions.[32] If the attached molecule can accept energy and/or electrons from the porphyrin, the increased electronic coupling leads to increased rates of energy and/or electron transfer.[24,33] For example, Hayes et al.[26] showed that a zinc porphyrin having a pyromellitimide electron acceptor attached to a meso phenyl group has a charge recombination rate that is 3 times faster than that of a porphyrin in which the acceptor is attached to a β-phenyl group.

(10) Johnson, D. G.; Niemczyk, M. P.; Minsek, D. W.; Wiederrecht, G. P.; Svec, W.; Gaines, G. L., III; Wasielewski, M. R. *J. Am. Chem. Soc.* **1993**, *115*, 5692−5701.
(11) Wiederrecht, G. P.; Niemczyk, M. P.; Svec, W.; Wasielewski, M. R. *J. Am. Chem. Soc.* **1996**, *118*, 81−88.
(12) Wasielewski, M. R.; Johnson, D. G.; Svec, W. A. *NATO ASI Ser., Ser. C* **1987**, *214*, 255−266.
(13) Holtzwarth, A. R.; Katterle, M.; Muller, M. G.; Ma, Y.-Z.; Prokhorenko, V. *Pure Appl. Chem.* **2001**, *73*, 469−474.
(14) Fukuzumi, S.; Ohkubo, K.; Imahori, H.; Shao, J.; Ou, Z.; Zheng, G.; Chen, Y.; Pandey, R. K.; Fujitsuka, M.; Ito, O.; Kadish, K. M. *J. Am. Chem. Soc.* **2001**, *123*, 10676−10683.
(15) Gust, D.; Moore, T. A.; Moore, A. L. *Acc. Chem. Res.* **2001**, *34*, 40−48.
(16) Jordens, S.; De Belder, G.; Lor, M.; Schweitzer, G.; Van der Auweraer, M.; Herrmann, A.; Wiesler, U. M.; Müllen, K.; De Schryver, F. C. *Photochem. Photobiol. Sci.* **2003**, *2003*, 1118−1124.
(17) Furuta, P.; Brooks, J.; Thompson, M. E.; Fréchet, J. M. *J. Am. Chem. Soc.* **2003**, *123*, 13165−13172.
(18) Aratani, N.; Osuka, A.; Cho, H. S.; Kim, D. J. *J. Photochem. Photobiol., C* **2002**, *3*, 25−52.
(19) Würthner, F.; Thalacker, C.; Diele, S.; Tschierske, C. *Chem. Eur. J.* **2001**, *7*, 2245−2253.
(20) Wagner, R. W.; Lindsey, J. S.; Seth, J.; Palaniappan, V.; Bocian, D. F. *J. Am. Chem. Soc.* **1996**, *118*, 3996−3997.
(21) Taniguchi, M.; Kim, H.-J.; Ra, D.; Schwartz, J. K.; Kirmaier, C.; Hindin, E.; Diers, J. R.; Prathapan, S.; Bocian, D. F.; Holten, D.; Lindsey, J. S. *J. Org. Chem.* **2002**, *67*, 7329−7342.
(22) Hindin, E.; Kirmaier, C.; Diers, J. R.; Tomizaki, K.-y.; Taniguchi, M.; Lindsey, J. S.; Bocian, D. F.; Holten, D. *J. Phys. Chem. B* **2004**, *108*, 8190−8200.
(23) Kirmaier, C.; Hindin, E.; Schwartz, J. K.; Sazanovich, I. V.; Diers, J. R.; Muthukumaran, K.; Taniguchi, M.; Bocian, D. F.; Lindsey, J. S.; Holten, D. *J. Phys. Chem. B* **2003**, *107*, 3443−3454.
(24) Holten, D.; Bocian, D. F.; Lindsey, J. S. *Acc. Chem. Res.* **2002**, *35*, 57−69.
(25) Redmore, N. P.; Rubtsov, I. V.; Therien, M. J. *J. Am. Chem. Soc.* **2003**, *125*, 8769−8778.
(26) Hayes, R. T.; Walsh, C. J.; Wasielewski, M. R. *J. Phys. Chem. A* **2004**, *108*, 2375−2381.
(27) Strachan, J.-P.; Gentemann, S.; Seth, J.; Kalsbeck, W. A.; Lindsey, J. S.; Holten, D.; Bocian, D. F. *J. Am. Chem. Soc.* **1997**, *119*, 11191−11201.
(28) Osuka, A.; Tanabe, N.; Kawabata, S.; Yamazaki, I.; Nishimura, Y. *J. Org. Chem.* **1995**, *60*, 7177−7185.
(29) Hopfield, J. J. *Proc. Natl. Acad. Sci. U.S.A.* **1974**, *71*, 3640−3644.
(30) Jortner, J. *J. Chem. Phys.* **1976**, *64*, 4860−4867.
(31) Marcus, R. *J. Chem. Phys.* **1984**, *81*, 4494−4500.
(32) Plato, M.; Moebius, K.; Michel-Beyerle, M. E.; Bixon, M.; Jortner, J. *J. Am. Chem. Soc.* **1988**, *110*, 7279−7285.
(33) Tsai, H.; Simpson, M. C. *Chem. Phys. Lett.* **2002**, *353*, 111−118.
(34) Gouterman, M. *Porphyrins* **1978**, *3*, 1−165.
(35) Weiss, C.; Kobayashi, H.; Gouterman, M. *J. Mol. Spectrosc.* **1965**, *16*, 415−450.
(36) Fajer, J.; Borg, D. C.; Forman, A.; Dolphin, D.; Felton, R. H. *J. Am. Chem. Soc.* **1970**, *92*, 3451−3459.
(37) Atamian, M.; Wagner, R. W.; Lindsey, J. S.; Bocian, D. F. *Inorg. Chem.* **1988**, *27*, 1510−1512.

Electronic structure calculations and electron−nuclear double-resonance (ENDOR) spectroscopy have shown that the electron density distributions within chlorins differ significantly from those of metalloporphyrins. Given the observed dependence of both energy- and electron-transfer rates on the detailed electron density distributions in porphyrins, it is important to carefully examine similar considerations for chlorins. Semiempirical molecular orbital calculations on the corresponding chlorin radical cations have predicted a modest 0.25 eV energy gap between the HOMO and HOMO−1 orbitals,[38] while ab initio calculations on the ethyl chlorophyllide *a* radical cation have estimated a 0.65 eV gap,[39] which is considerably larger than that observed in metalloporphyrins. However, more recently, O'Malley et al.[40] reported density functional theory (DFT) calculations on chlorophyll cations with water-ligated metal centers that give a gap of only ∼0.03 eV between these orbitals. Direct measurements of the spin density distributions in the radical cations of Chl *a* and several of its derivatives using ENDOR spectroscopy show high spin densities at the β carbon atoms of the pyrroles, whereas the spin densities at the meso positions, in particular the 20-position, are relatively low.[38,41−43] This electron density distribution is very similar to that of metalloporphyrins having β alkyl substituents in which the a_{1u} orbital is the HOMO. Mössler et al.[44] have reported ENDOR spectra of a series zinc *meso*-tetraphenylchlorins in which one phenyl was either converted into a benzoquinone electron acceptor or replaced by a 1,4-cyclohexyl group bearing the benzoquinone. In particular, they studied the system in which the quinone or cyclohexylquinone occupies the 20-position of the macrocycle. They found that the attachment of these groups to the macrocycle did not significantly perturb the spin (and charge) distribution in the chemically generated radical cation. The only observed effects were small changes in the dihedral angles of the β-protons on the reduced ring, which resulted in changes in the hyperfine coupling constants (hfcc's) of these protons.

In this study we report the synthesis and photophysics of three donor−acceptor dyads in which arylene bis(dicarboximide) acceptors are attached to the 20-position of chlorophyll donors via phenyl groups (Figure 1). The benefits of using arylene bis(dicarboximide)s as electron acceptors in self-assembling systems have been discussed recently.[45−48] The attachment of an arylene bis(dicarboximide) acceptor directly to the 20-position of the chlorin macrocycle would not only preserve the ability of the chlorin to direct aggregation along its ring A−ring C axis but also enhance the self-association of the dyads by adding an additional $\pi-\pi$ interaction. Arylene bis(dicarboximide)s are easy to reduce, yielding stable radical anions with intense and distinct electronic transitions that make them easy to identify in transient optical experiments.[45−50] PDIs have proven to be excellent complementary chromophores for porphyrin-based systems by filling the spectral gap between the Soret and Q bands, thus serving as a light-harvesting component of the system.[50] The PDI chromophore should prove even more useful in a chlorophyll-based system, since the intense Chl *a* Q_y band is shifted ∼100 nm to the red of the lowest electronic transition in metalloporphyrins.

For comparison, an analogous group of three porphyrin-containing donor−acceptor dyads was synthesized and characterized. The zinc 5,10,15-tri(*n*-pentyl)-20-phenylporphyrin was chosen to match both the single phenyl linkage to the acceptor and the free energy for charge recombination relative to that of the chlorophyll series. The photophysical studies presented here are conducted on the monomeric, disaggregated state of the dyads and will be compared to the aggregated systems in a subsequent publication. We also characterize the spin density distribution in the radical cation of this new arylated chlorin using ENDOR spectroscopy in fluid solution to probe the influence of the 20-phenyl group on the structure of the radical cation and its electronic coupling to the reduced acceptor. To explain the results of the photophysical and ENDOR studies, a series of DFT calculations were performed on both chlorin and porphyrin model systems.

Experimental Section

Synthesis. The syntheses of zinc methyl 3-ethyl-20-phenylpyrochlorophyllide *a* (**4**, ZCPh) and the donor−acceptor dyads having arylenebis(dicarboximide)s attached to the corresponding 20-(*p*-aminophenyl) derivative (**9**, ZCPh-NI; **10**, ZCPh-PDIa; and **11**, ZCPh-PDIb), as well as the intermediates leading to them, are detailed in the Supporting Information. The syntheses of zinc 5-phenyl-10,15,20-tri(*n*-pentyl)porphyrin (**13**, Z3PnPh) and its corresponding 20-aminophenyl derivatives (**19**, Z3PnPh-NI; **20**, Z3PnPh-PDIa; and **21**, Z3PnPh-PDIb) used for comparisons to the chlorophyll derivatives are also detailed in the Supporting Information. Each chlorin was synthesized from chlorophyll *a*, which was extracted from the alga *Spirulina maxima* and subsequently converted to methyl 3-ethylpyropheophorbide *a* using literature procedures.[51,52] The porphyrins were produced from pyrrole and the appropriate aldehydes using the Lindsey method.[53] Characterization was performed with Varian 400 MHz NMR and PE Voyager DE-Pro MALDI-TOF mass spectrometers. High-resolution electrospray and fast atom bombardment mass spectra were obtained with the 70-SE-4F and Q-Tof Ultima mass spectrometers at the University of Illinois at Champaign-Urbana.

Electrochemistry. Electrochemical measurements were performed using a CH Instruments model 622 electrochemical workstation. Reversible, half-wave potentials were determined in butyronitrile (PrCN) containing 0.1 M n-$Bu_4N^+BF_4^-$ electrolyte. A 1.0-mm-diameter platinum disk electrode, platinum wire counter electrode, and Ag/Ag_xO reference electrode were employed. Ferrocene/ferrocenium (Fc/Fc^+, 0.52 V vs SCE) was used as an internal reference for all measurements.

(38) Davis, M. S.; Forman, A.; Fajer, J. *Proc. Natl. Acad. Sci. U.S.A.* **1979**, *76*, 4170−4174.
(39) Petke, J. D.; Maggiora, G. M.; Shipman, L. L.; Christoffersen, R. E. *Photochem. Photobiol.* **1980**, *31*, 243−257.
(40) O'Malley, P. J.; Collins, S. J. *J. Am. Chem. Soc.* **2001**, *123*, 11042−11046.
(41) Norris, J. R.; Scheer, H.; Druyan, M. E.; Katz, J. J. *Proc. Natl. Acad. Sci. U.S.A.* **1974**, *71*, 4897−4900.
(42) Scheer, H.; Katz, J. J.; Norris, J. R. *J. Am. Chem. Soc.* **1977**, *99*, 1372−1381.
(43) Käss, H.; Lubitz, W.; Hartwig, G.; Scheer, H.; Noy, D.; Scherz, A. *Spectrochim. Acta, Part A* **1998**, *54A*, 1141−1156.
(44) Mössler, H.; Wittenberg, M.; Niethammer, D.; Mudrassagam, R. K.; Kurreck, H.; Huber, M. *Magn. Reson. Chem.* **2000**, *38*, 67−84.
(45) Rybtchinski, B.; Sinks, L. E.; Wasielewski, M. R. *J. Phys. Chem. A* **2004**, *108*, 7497−7505.
(46) Rybtchinski, B.; Sinks, L. E.; Wasielewski, M. R. *J. Am. Chem. Soc.* **2004**, *126*, 12268−12269.
(47) Ahrens, M. J.; Sinks, L. E.; Rybtchinski, B.; Liu, W.; Jones, B. A.; Giaimo, J. M.; Gusev, A. V.; Goshe, A. J.; Tiede, D. M.; Wasielewski, M. R. *J. Am. Chem. Soc.* **2004**, *126*, 8284−8294.
(48) van der Boom, T.; Hayes, R. T.; Zhao, Y.; Bushard, P. J.; Weiss, E. A.; Wasielewski, M. R. *J. Am. Chem. Soc.* **2002**, *124*, 9582−9590.
(49) Gosztola, D.; Niemczyk, M. P.; Svec, W.; Lukas, A. S.; Wasielewski, M. R. *J. Phys. Chem. A* **2000**, *104*, 6546−6551.
(50) Prathapan, S.; Yang, S. I.; Seth, J.; Miller, M. A.; Bocian, D. F.; Holten, D.; Lindsey, J. S. *J. Phys. Chem. B* **2001**, *105*, 8237−8248.
(51) Smith, K. M.; Goff, D. A.; Simpson, D. J. *J. Am. Chem. Soc.* **1985**, *107*, 4946−4954.
(52) Kenner, G. W.; McCombie, S. W.; Smith, K. M. *J. Chem. Soc., Perkin Trans. 1* **1973**, 2517−2523.
(53) Lindsey, J. S.; Schreiman, I. C.; Hsu, H. C.; Kearney, P. C.; Marguerettaz, A. M. *J. Org. Chem.* **1987**, *52*, 827−836.

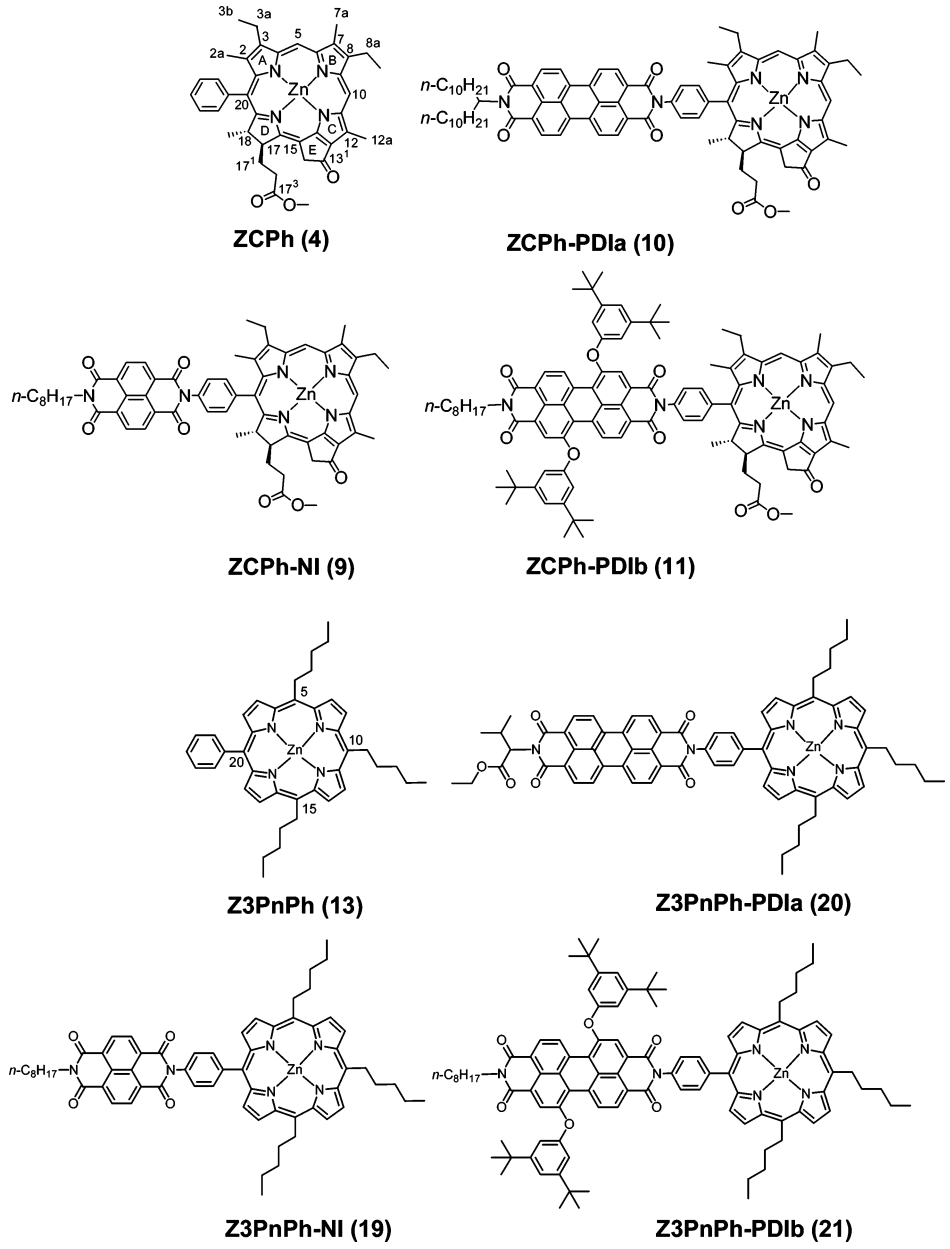

Figure 1. Structures of molecules studied here.

Optical Spectroscopy. UV−vis absorption measurements were made on a Shimadzu spectrometer (UV1601). Steady-state fluorescence measurements were made on a single-photon-counting fluorimeter (PTI). All measurements were performed at room temperature. Optical densities of the solutions were kept below 0.1 at 655 nm in a 1-cm cuvette, and excitation/emission geometry was at right angles. Toluene was purified by passing it through a series of CuO and alumina columns, while tetrahydrofuran (THF) was purified by passing it through two alumina columns (GlassContour) immediately prior to use.

Femtosecond transient absorption measurements were made with a Ti:sapphire laser system as detailed in the Supporting Information. The instrument response function (IRF) for the pump−probe experiments was 150 fs. Typically 5 s of averaging was used to obtain the transient spectrum at a given delay time. Cuvettes with a 2 mm path length were used, and the samples were irradiated with 0.5 μJ/pulse focused to a 200-μm spot. The optical density at λ_{ex} was kept between 0.2 and 0.4 to prevent aggregation. Analysis of the kinetic data was performed at multiple wavelengths using a Levenberg−Marquardt nonlinear least-squares fit to a general sum-of-exponentials function with an added Gaussian to account for the finite instrument response.

Fluorescence lifetimes were determined using a frequency-doubled, cavity-dumped Ti:sapphire laser as the excitation source and a Hamamatsu C4780 picosecond fluorescence lifetime measurement system as described in the Supporting Information. The energy of the 400 nm, 25 fs pulses was attenuated to approximately 1.0 nJ/pulse for all fluorescence lifetime experiments. The total IRF of the streak camera system was 25 ps. The samples were prepared in glass cuvettes, and the optical density at the excitation wavelength was typically 0.020−0.035. At λ_{max} of the samples, the optical density was typically 0.080−0.105. All fluorescence data were acquired in single-photon-counting mode using the Hamamatsu HPD-TA software. The data were fit using the Hamamatsu fitting module and deconvoluted using the laser pulse profile. Measurements were generally repeated three times and the resulting time constants were averaged. Deviation from the mean was generally no worse than ±5%.

EPR and ENDOR Spectroscopy. All samples and solvents were handled in an inert atmosphere glovebox (MBraun Unilab). Stock solutions of ZC, ZCPh, and the I_2 oxidant were prepared in dry CH_2Cl_2/THF (9:1 v/v). Solutions of the ZC and ZCPh radical cations were formed by oxidation with a 10- or 20-fold excess (mol/mol) of I_2. The

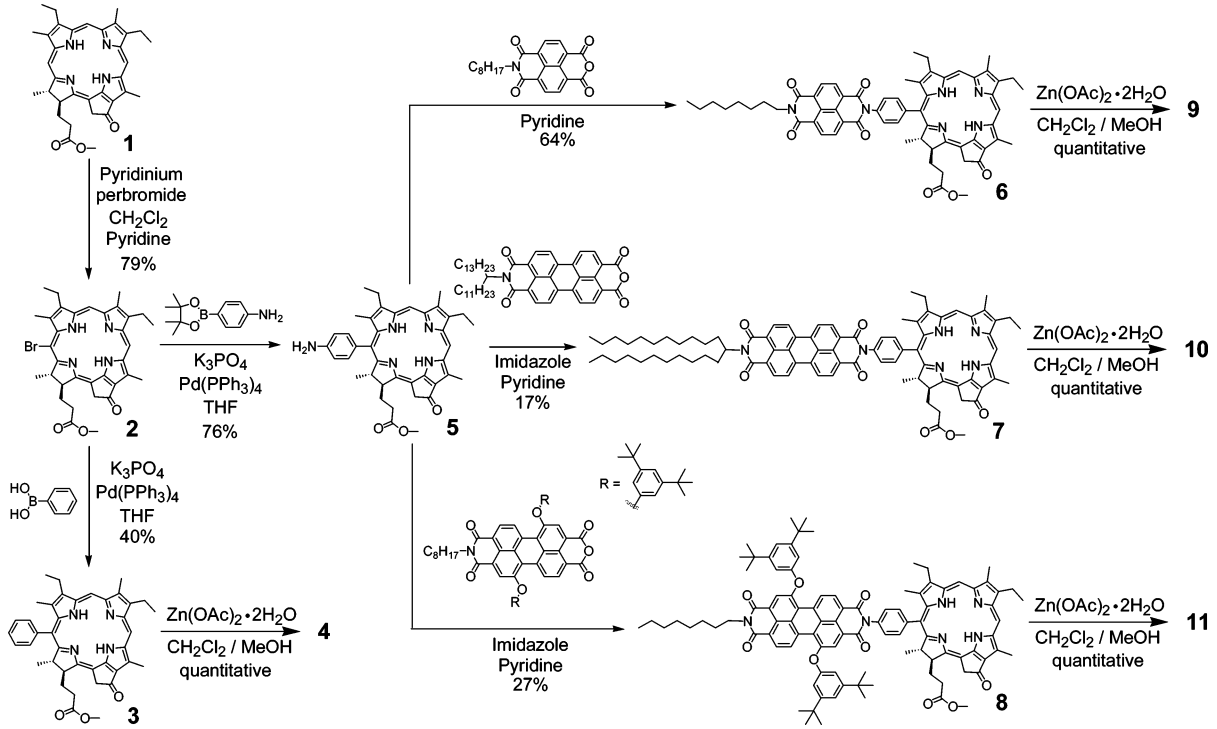

Figure 2. Synthetic scheme.

resulting 0.5 mM samples of oxidized chlorins were then loaded into 1.4- and 2.4-mm-i.d. quartz tubes and frozen in liquid nitrogen pending analysis. EPR and ENDOR spectra were acquired with a Bruker ELEXSYS E580 spectrometer, fitted with the DICE ENDOR accessory, EN801 resonator, and radio frequency (RF) power amplifier (ENI A-500). Applied RF powers ranged from 180 to 700 W across the 20 MHz scanned range, and microwave power was typically 31 mW. The sample temperature was controlled by a liquid nitrogen flow system, and spectra were obtained at 170, 195, and 220 K.

Computational Methods. Geometry optimizations of compounds **4** and **13** in both their neutral and cationic states were performed using Gaussian 03[54] using the Perdew−Wang 1991 nonlocal functional[55] with the 6-31G* basis set. No symmetry constraints were enforced, and all open-shell calculations were performed using unrestricted methods. The spin contamination in the radical species was found to deviate from the expected value by less than 5% (calculated $\langle S^2 \rangle \leq 0.78$; expected, 0.75). Single-point calculations used to determine internal reorganization energies and the effects of bis(dicarboximide) radical anions on the electronic structures of $ZCPh^{+\bullet}$ and $Z3PnPh^{+\bullet}$ were performed using the above geometry-optimized structures. The locations of the partial negative point charges relative to the cationic macrocycles were determined from geometry-optimized neutral structures of models containing the bis(dicarboximide) acceptors (not shown).

Results

Synthesis. The syntheses of **4** and **9**−**11** are outlined in Figure 2. Chlorophyll *a* was extracted from the alga *Spirulina maxima* and subsequently converted to methyl 3-ethylpyropheophorbide *a* (**1**) according to known procedures.[51] Selective bromination of the 20-position of **1** results in the formation of the bromo compound **2**.[52] Suzuki cross-coupling of **2** with phenylboronic acid using the mild conditions outlined by Shi and Boyle[56] for use with free-base porphyrins resulted in the formation of the 20-phenyl derivative **3** in 40% yield, while the analogous reaction of **2** with the pinacol ester of *p*-aminophenylboronic acid gave the 20-(*p*-aminophenyl) derivative **5** in 76% yield. The arylene monoimide monoanhydride precursors to the NI, PDIa, and PDIb electron acceptors were then condensed with the amine in **5** to yield the corresponding arylene bis(dicarboximide) dyads **6**−**8**.[11,47,57] Finally, the free-base pheophorbides **3** and **6**−**8** were metalated using zinc acetate in CH_2Cl_2/CH_3OH to give the corresponding zinc chlorophyllides, **4** and **9**−**11**. For spectroscopic comparisons to the chlorophyll derivatives, an analogous set of porphyrins was prepared. The syntheses of the porphyrin derivatives are outlined in Figure S1 in the Supporting Information. 5-Phenyl-10,15,-20-tri(*n*-pentyl)porphyrin (**12**) and the corresponding 20-(*p*-nitrophenyl) derivative **14** were prepared by a mixed condensation of *n*-hexanal with either benzaldehyde or *p*-nitrobenzaldehyde, respectively, using Lindsey's method.[53] Reduction of the nitro group in **14** gave the 20-(*p*-aminophenyl) derivative **15** in 73% yield. Condensation of **15** with the arylene monoimide monoanhydride precursors to the NI, PDIa, and PDIb electron acceptors gave free-base porphyrin acceptors **16**−**18**. The free-base porphyrins **12** and **16**−**18** were metalated using zinc acetate in CH_2Cl_2/CH_3OH to give the corresponding zinc porphyrins, **13** and **19**−**21**.

Steady-State Spectroscopy. The UV−vis spectra of the ZCPh series of donor−acceptor dyads are compared to the spectrum of ZCPh in toluene in Figure 3, while the corresponding spectra of the Z3PnPh series of dyads are compared to the spectrum of Z3PnPh in Figure 4. The corresponding spectra obtained in THF (Figures S2 and S3) are nearly identical. In the ZCPh spectra, the chlorin Soret bands occur at 428 nm and

(54) Frisch, M. J.; et al. *Gaussian*; Gaussian, Inc.: Wallingford, CT, 2004.
(55) Perdew, J. P.; Chevary, J. A.; Vosko, S. H.; Jackson, K. A.; Pederson, M. R.; Singh, D. J.; Fiolhais, C. *Phys. Rev. B: Condens. Matter Mater. Phys.* **1992**, *46*, 6671−6687.
(56) Shi, B.; Boyle, R. W. *J. Chem. Soc., Perkin Trans. 1* **2002**, *11*, 1397−1400.
(57) Holman, M. W.; Liu, R.; Adams, D. M. *J. Am. Chem. Soc.* **2003**, *125*, 12649−12654.

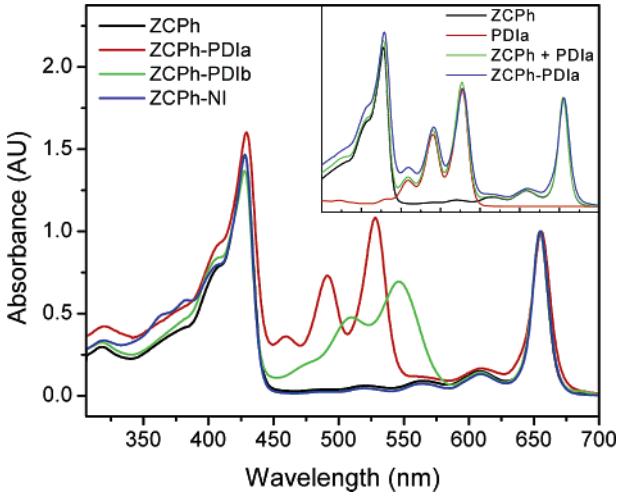

Figure 3. Ground-state electronic absorption spectra of the indicated compounds in toluene. Inset: The spectrum of ZCPh-PDIa together with the spectra of its component chromophores and the simple sum of these spectra.

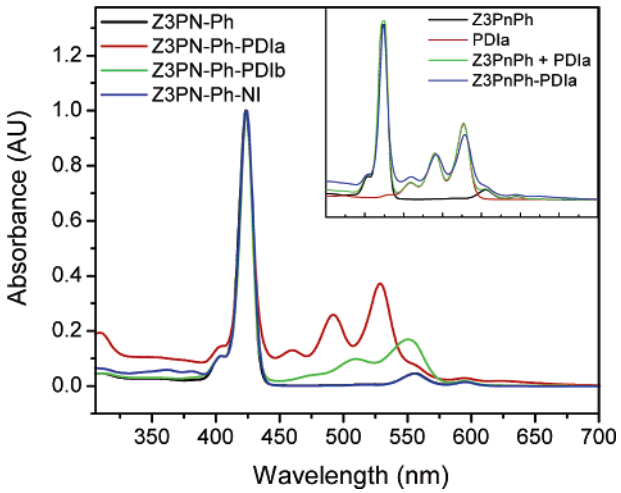

Figure 4. Ground-state electronic absorption spectra of the indicated compounds in toluene. Inset: The spectrum of Z3PnPh-PDIa together with the spectra of its component chromophores and the simple sum of these spectra.

the $Q_x(0,1)$, $Q_x(0,0)$, $Q_y(0,1)$, and $Q_y(0,0)$ bands at 521, 564, 609, and 655 nm, respectively. In the porphyrin spectra, the porphyrin Soret bands appear at 424 nm and the $Q_y(0,1)$ and $Q_y(0,0)$ bands at 556 and 595 nm, respectively. The ground-state absorption spectra of both ZCPh and Z3PnPh are essentially unperturbed by the attachment of either of the three electron acceptors at the para position of the 20-phenyl group. The spectra of ZCPh-NI and Z3PnPh-NI contain additional peaks at 361 and 381 nm due to the NI acceptors, while in ZCPh-PDIa, Z3PnPh-PDIa, ZCPh-PDIb, and Z3PnPh-PDIb, the visible spectra between 450 and 600 nm exhibit absorption features of the PDI derivatives. Local maxima for PDIa appear at 459, 491, and 528 nm and for PDIb at 479, 510, and 546 nm.[47,49] Deviations in the absorption features exhibited by both donors in the 350−400 nm region are due to lower intensity transitions in the PDIa and PDIb chromophores.[47,49] Since the spectra of the covalently linked systems can be closely approximated using a weighted sum of the component absorptions (Figures 3 and 4 insets and Figure S4), only weak ground-state electronic interactions occur between all redox pairs.[58]

The fluorescence maxima and quantum yields for both the ZCPh and Z3PnPh series of donor−acceptor dyads as well as those of reference compounds ZCPh, zinc methyl 3-ethylpyrochlorophyllide *a* (Zn EtPChlide *a*), and Z3PnPh in toluene and THF are presented in Table 1. The values obtained in THF are nearly identical to those given for toluene. For all molecules, the emission features are approximately mirror images of the corresponding $Q_y(0,0)$ and $Q_y(0,1)$ absorption features. The fluorescence quantum yield of ZCPh is only slightly lower than that of Zn EtPChlide *a*.[59] The fluorescence of all molecules with the arylene bis(dicarboximide) electron acceptors attached is significantly quenched, suggesting that electron transfer occurs in these molecules (see below).

Energetics. The one-electron oxidation and reduction potentials for both the ZCPh and Z3PnPh series of donor−acceptor dyads as well as those of several reference compounds are summarized in Table 2. Neither the oxidation potentials of the donors nor the reduction potentials of the acceptors used to construct the dyads are significantly affected by covalent linkages between the two redox-active centers. The redox potentials of the acceptors change only slightly when they are linked to the chlorin or porphyrin donor, in accord with small substituent effects observed earlier.[60] The electrochemical data reinforces the conclusion suggested by the UV−vis spectra that the ground-state electronic interactions between the donor and acceptors are weak.

The energies of the radical pair states for the donor−acceptor dyads were calculated using the experimentally determined redox potentials along with computed ionic radii and donor−acceptor distances. The ion-pair distances and ionic radii were estimated using MM^+ geometry-optimized models (Table S1, Supporting Information).[61] Equation 1 yields estimates of the energies of the solvated ion pairs based on the Born dielectric continuum model of solvent,[62]

$$\Delta G_{IP} = E_{OX} - E_{RED} - \frac{e^2}{r_{DA}\epsilon_S} + e^2\left(\frac{1}{2r_D} + \frac{1}{2r_A}\right)\left(\frac{1}{\epsilon_S} - \frac{1}{\epsilon_{SP}}\right) \quad (1)$$

where E_{OX} and E_{RED} are the redox potentials of the donor and acceptor, respectively, determined in a polar solvent with dielectric constant ϵ_{SP}, ϵ_S is the dielectric constant of the solvent in which the electron transfer takes place, r_D and r_A are the ionic radii, and r_{DA} is the donor−acceptor distance. The free energies for charge separation and charge recombination, ΔG_{CS} and ΔG_{CR}, respectively (see Table 3), were then determined using eqs 2 and 3.

$$\Delta G_{CS} = \Delta G_{IP} - E_{S1} \quad (2)$$

$$\Delta G_{CR} = -\Delta G_{IP} \quad (3)$$

The lowest excited-state energies (E_{S1}) for the dyads were

(58) Greenfield, S. R.; Svec, W.; Gosztola, D.; Wasielewski, M. R. *J. Am. Chem. Soc.* **1996**, *118*, 6767−6777.
(59) Wasielewski, M. R.; Johnson, D. G.; Niemczyk, M. P.; Gaines, G. L., III; O'Neil, M. P.; Svec, W. *J. Am. Chem. Soc.* **1990**, *112*, 6482−6488.
(60) Viehbeck, A.; Goldberg, M. J.; Kovac, C. A. *J. Electrochem. Soc.* **1990**, *137*, 1460−1466.
(61) Hyperchem, MM+, and PM3 calculations were performed using Hyperchem software from Hypercube, Inc., 115 NW 1114th St., Gainesville, FL 32601.
(62) Weller, A. *Z. Phys. Chem.* **1982**, *133*, 93−98.

Table 1. UV−Vis Absorption and Emission

	toluene				THF			
compd	λ_{abs}[a]	λ_{em}[b]	E_S[c]	Φ_F[d]	λ_{abs}[a]	λ_{em}[b]	E_S[c]	Φ_F[d]
Zn EtPChlide *a*	657	662	1.88	0.15	657	662	1.88	0.15
ZCPh	656	658	1.89	0.13	653	657	1.89	0.15
ZCPh-NI	655	658	1.89	<0.0005	654	657	1.89	<0.0005
ZCPh-PDIa	655	658	1.89	<0.0005	654	657	1.89	<0.0005
ZCPh-PDIb	655	658	1.89	<0.0005	654	657	1.89	<0.0005
Z3PnPh	595	605	2.07	0.03	603	610	2.05	0.03
Z3PnPh-NI	595	605	2.07	<0.0005	603	610	2.05	<0.0005
Z3PnPh-PDIa	595	605	2.07	<0.0005	603	610	2.05	<0.0005
Z3PnPh-PDIb	595	605	2.07	<0.0005	603	610	2.05	<0.0005

[a] Ground-state absorption maxima corresponding to the $Q_y(0,0)$ band. [b] Steady-state fluorescence maxima following 638 (ZCPh) and 550 nm (Z3PnPh) excitation. [c] First singlet excited-state energies calculated using the average energies of the absorption and emission maxima. [d] Fluorescence quantum yields of ZCPh derivatives use Zn EtPChlide *a* as a reference, while those of Z3PnPh derivatives use ZnTPP as reference.

Table 2. Redox Potentials (V vs SCE)[a]

comps	E_{OX}	E_{RED}
ZCPh-NI	0.66	−0.51
ZCPh-PDIa	0.66	−0.45
ZCPh-PDIb	0.66	−0.55
Z3PnPh-NI	0.65	−0.51
Z3PnPh-PDIa	0.65	−0.45
Z3PnPh-PDIb	0.65	−0.55

[a] All values obtained in PrCN/0.1 M $TBABF_4$.

derived from the average energy of the $Q_y(0,0)$ absorption and fluorescence maxima of the respective porphyrin or chlorophyll donor (Table 1).[58] Equations 1 and 2 predict that photoinduced charge separation should occur in all six dyads in both toluene and THF.

Transient Absorption Spectroscopy. Excitation of ZCPh in toluene with 655 nm, 120 fs pulses yields the transient absorption spectrum of ^{1}*ZCPh within the 150 fs instrument response function of the apparatus (Figure 5). The bleach of the $Q_y(0,0)$ band occurs at 655 nm, while ^{1}*ZCPh has a broad absorption between 440 and 640 nm with local maxima occurring at 455, 587, and 629 nm. Stimulated emission from ^{1}*ZCPh can be detected as a negative feature centered around 723 nm. Transient absorption kinetics monitored at 631 and 659 nm (inset to Figure 5) show complex decays over the 5 ns time window as ^{1}*ZCPh decays competitively to ground state and the long-lived ^{3}*ZCPh. The corresponding spectra and kinetics for ZCPh in THF are given in Figure S5. The lifetimes of ^{1}*ZCPh in toluene (τ = 3.2 ns) and THF (τ = 4.0 ns) were determined independently from its fluorescence decay (not shown). Excitation of ZCPh into its second excited state (S_2) using 414 nm, 120 fs pulses, followed by rapid, instrument-limited internal conversion, produces transient absorption spectra identical to those attained using 655 nm excitation (not shown).

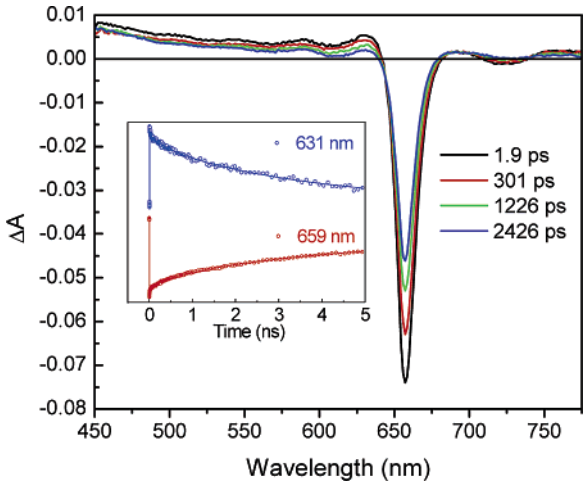

Figure 5. Transient absorption spectra of ZCPh in toluene following excitation with 655 nm, 120 fs laser pulses. Inset: Transient absorption kinetics for ZCPh (blue) at 631 nm and (red) at 659 nm. Nonlinear least-squares fits to the data are also shown.

Attachment of arylene bis(dicarboximide)s to ZCPh provides an efficient, nonradiative deactivation pathway for the ^{1}*ZCPh excited state. Thus, the transient spectra in Figure 6 confirm the initial formation of ^{1}*ZCPh (features at 440−640 nm), while the growth of the sharp $NI^{-\bullet}$ absorption band at 475 nm[49] indicates that the radical ion pair $ZCPh^{+\bullet}$−$NI^{-\bullet}$ is formed. Kinetic traces obtained at 478 and 657 nm (inset to Figure 6) reveal the time constants for charge separation (τ_{CS}) leading to

Table 3. Charge Separation and Charge Recombination Data

compd	τ_{CS} (ps)	ΔG_{CS} (eV)	V_{CS} (cm^{-1})	τ_{CR} (ps)	ΔG_{CR} (eV)	V_{CR} (cm^{-1})
			Toluene			
ZCPh-NI	21 ± 2	−0.31	31	1150 ± 50	−1.58	88
ZCPh-PDIa	12 ± 1	−0.43	17	2000 ± 200	−1.46	36
ZCPh-PDIb	25 ± 1	−0.33	22	3300 ± 200	−1.56	25
Z3PnPh-NI	16 ± 1	−0.50	47	1100 ± 100	−1.57	116
Z3PnPh-PDIa	14 ± 2	−0.62	22	1850 ± 50	−1.45	65
Z3PnPh-PDIb	19 ± 1	−0.52	31	3050 ± 50	−1.55	32
			THF			
ZCPh-NI	13 ± 1	−0.66	23	25 ± 2	−1.23	54
ZCPh-PDIa	14 ± 1	−0.73	21	31 ± 2	−1.16	37
ZCPh-PDIb	19 ± 1	−0.63	20	43 ± 2	−1.26	46
Z3PnPh-NI	5 ± 1	−0.82	42	18 ± 1	−1.25	99
Z3PnPh-PDIa	7 ± 2	−0.90	42	24 ± 2	−1.17	60
Z3PnPh-PDIb	9 ± 1	−0.80	31	37 ± 2	−1.27	76

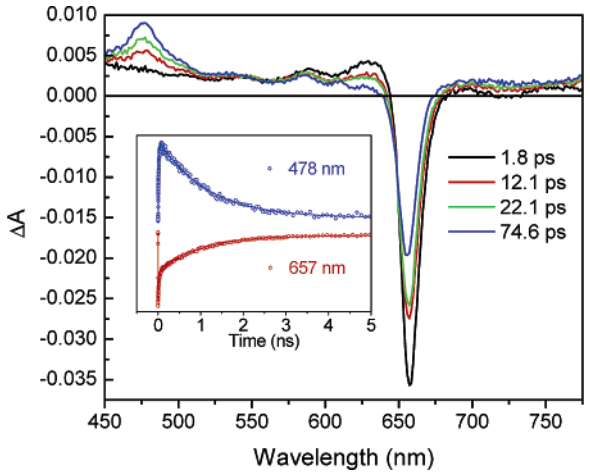

Figure 6. Transient absorption spectra of ZCPh-NI in toluene following excitation with 655 nm, 120 fs laser pulses. Inset: Transient absorption kinetics for ZCPh-NI (blue) at 478 nm and (red) at 657 nm. Nonlinear least-squares fits to the data are also shown.

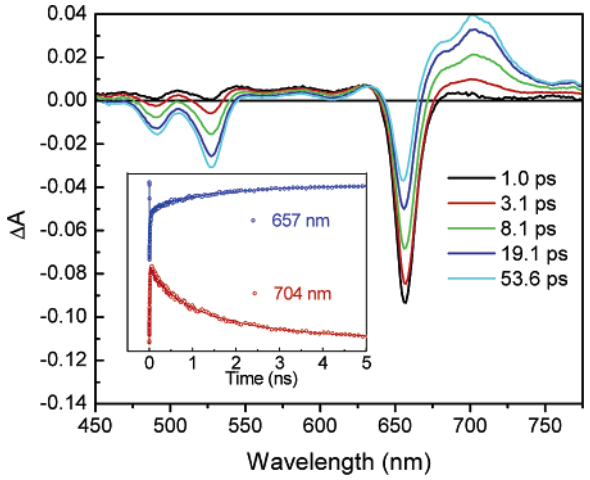

Figure 7. Transient absorption spectra of ZCPh-PDIa in toluene following excitation with 655 nm, 120 fs laser pulses. Inset: Transient absorption kinetics for ZCPh-PDIa (blue) at 657 nm and (red) at 704 nm. Nonlinear least-squares fits to the data are also shown.

$ZCPh^{+\bullet}-NI^{-\bullet}$ and its subsequent recombination (τ_{CR}) (Table 3). The ZCPh-PDIa and ZCPh-PDIb dyads have donors (ZC) and acceptors (PDI) that both absorb in the visible, resulting in complex transient absorption spectra. Selective excitation of the chlorin within ZCPh-PDIa in toluene using 655 nm, 120 fs pulses results in the transient absorption spectra shown in Figure 7. The initial spectrum due to ^{1}*ZCPh evolves in time to that of $ZCPh^{+\bullet}$-$PDIa^{-\bullet}$, which is comprised of ground-state bleaches of PDI at 491 and 527 nm and ZC at 657 nm as well as the appearance of an absorption at 701 nm due to the formation of $PDIa^{-\bullet}$.[49] The kinetic data obtained in toluene near these wavelengths are shown in the inset to Figure 7 and are given in Table 3. The electron-accepting PDIb chromophore is functionalized with 3,5-di-*tert*-butylphenoxy groups, which enhance the solubility of the PDI core and result in a one-electron reduction potential that is 0.1 V more negative than that of PDIa. In addition, the electronic absorption spectra of both the ground state and radical anion of PDIb are red-shifted and broadened relative to those of PDIa.[47] The radical pair state, $ZCPh^{+\bullet}-PDIb^{-\bullet}$, is obtained following selective excitation of ZC using 655 nm, 120 fs laser pulses (Figure 8). The PDIb

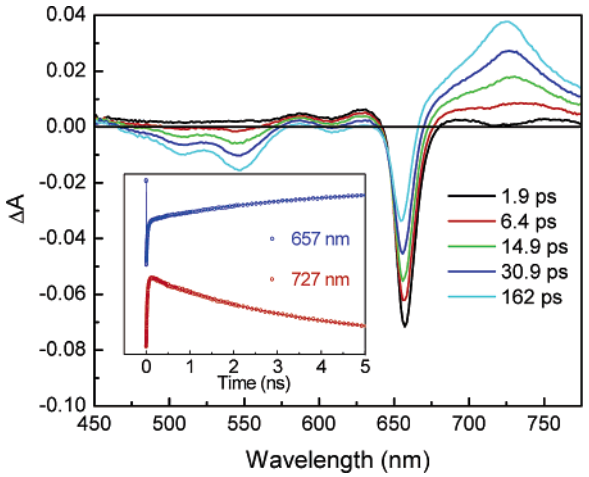

Figure 8. Transient absorption spectra of ZCPh-PDIb in toluene following excitation with 655 nm, 120 fs laser pulses. Inset: Transient absorption kinetics for ZCPh-PDIb (blue) at 657 nm and (red) at 727 nm. Nonlinear least-squares fits to the data are also shown.

ground-state bleaches occur at 510 and 546 nm, and the $PDI^{-\bullet}$ absorption feature occurs at 725 nm. Kinetic data monitored at 657 and 727 nm (inset to Figure 8 and Table 3) give the rates of charge separation and recombination. An analogous set of transient absorption data obtained for ZCPh-NI, ZCPh-PDIa, and ZCPh-PDIb in THF (Figures S6−S8) shows spectra similar to those obtained in toluene. Charge separation and recombination time constants in THF are presented in Table 3. As expected, in the more polar solvent the time constants for both charge separation and recombination are faster than those observed in toluene.

Excitation of Z3PnPh with 414 nm, 120 fs pulses yields ^{1}*Z3PnPh, following rapid, instrument-limited relaxation from the second singlet excited state (S_2). The major features include broad absorptions at 450−550 and 575−720 nm as well as ground-state bleaching of the $Q_y(0,1)$ and $Q_y(0,0)$ bands at 564 and 595 nm, respectively (Figures S9 (toluene) and S10 (THF)). Once again, due to the complexity of the transient absorption decay of ^{1}*Z3PnPh over the limited 5 ns time window, the lifetimes of ^{1}*Z3PnPh in toluene (τ = 2.3 ns) and THF (τ = 1.9 ns) were determined from its fluorescence decay (not shown). ^{1}*Z3PnPh can also be directly accessed using 595 nm pulses as evidenced by acquisition of transient absorption spectra identical to those attained using 414 nm excitation (not shown).

Attachment of arylene bis(dicarboximide)s to Z3PnPh also provides efficient, nonradiative deactivation pathways for the ^{1}*Z3PnPh excited state. Selective excitation of the metalloporphyrin within Z3PnPh-NI, Z3PnPh-PDIa, and Z3PnPh-PDIb in toluene using 414 nm, 120 fs pulses results in the transient absorption spectra shown in Figures S11−S13. The only significant difference between these transient absorption spectra and those of the ZCPh dyads is the position and intensity of the ground-state bleaches due to Z3PnPh (see above). The kinetic data obtained in toluene at wavelengths corresponding to the radical anion absorbance maxima and ground-state bleach minima for the three donor−acceptor dyads are shown in the insets of Figures S11−S13, and the values are listed in Table 3. An analogous set of transient absorption data obtained for Z3PnPh-NI, Z3PnPh-PDIa, and Z3PnPh-PDIb in THF shows spectra similar to those obtained in toluene (Figures S14−S16). Charge separation and recombination time constants in THF

are presented in Table 3. Once again, in the more polar solvent the time constants for both charge separation and recombination are faster than those observed in toluene.

The PDI electron acceptors serve as excellent antenna chromophores for both ZC and Z3PnP by absorbing light in the spectral window between the Soret and Q bands of these macrocycles and efficiently funneling excitation energy to them. Ultrafast energy transfer from the PDI derivatives in ZCPh-PDIa, ZCPh-PDIb, Z3PnPh-PDIa, and Z3PnPh-PDIb to the electron donors, ZC and Z3PnPh, is demonstrated by selective excitation of the PDI chromophores using 510 nm, 120 fs laser pulses. In ZCPh-PDIa and Z3PnPh-PDIa, excitation of PDIa in toluene results in the instrument-limited appearance of ^{1*}PDIa, as evidenced by concurrent bleaching of the 491 and 527 nm ground-state absorption bands and the growth of the excited-state feature centered at 690 nm. Decays of the transient spectral features of PDIa, monitored at 526 and 706 nm, respectively, reveal that energy transfer occurs with $\tau_{EnT} = 400$ fs in ZCPh-PDIa (Figure S17) and $\tau_{EnT} = 550$ fs in Z3PnPh-PDIa (Figure S18). Energy transfer in ZCPh-PDIb and Z3PnPh-PDIb occurs with similar time constants, $\tau_{EnT} = 350$ (Figure S19) and 500 fs (Figure S20), respectively, as determined by monitoring their transient absorption features at 507 and 729 nm. The lifetime of the lowest excited singlet state of both isolated PDI chromophores is $\tau = 4.5$ ns with a fluorescence quantum yield of unity.[48] Given that the lifetime of ^{1*}PDI is approximately 3 orders of magnitude longer than the experimentally determined energy-transfer rates, energy transfer from PDIa or PDIb to ZC and Z3PnP occurs with a quantum yield of unity. Following energy transfer, ZCPh-PDIa, ZCPh-PDIb, Z3PnPh-PDIa, and Z3PnPh-PDIb each undergo electron transfer with the same rates obtained by selective photoexcitation of either ZCPh or Z3PnPh with 150 fs laser pulses tuned to their respective absorbance maxima.

ENDOR Spectroscopy. The CW-EPR spectra of $ZC^{+\bullet}$ and $ZCPh^{+\bullet}$ are inhomogeneously broadened due to the large number of hfcc's, resulting in a single unresolved line for each spectrum (not shown). Isotropic hfcc's were obtained from ENDOR spectroscopy in liquid CH_2Cl_2/THF solution using the ENDOR resonance condition $\nu^{\pm}_{ENDOR} = |\nu_n \pm a/2|$, where $\nu^{\pm}_{ENDOR}$ are the ENDOR transition frequencies, ν_n is the proton Larmor frequency, and a is the isotropic hfcc.[63] The ENDOR spectra of $ZC^{+\bullet}$ and $ZCPh^{+\bullet}$ obtained at 195 K are presented in Figure 9. The $ZC^{+\bullet}$ spectrum shows six well-defined peak pairs, and the $ZCPh^{+\bullet}$ spectrum shows five. The assignments listed in Table 4 are based on previous studies of a series of substituted chlorophyll radical cations, including pyro-Chl $a^{+\bullet}$, whose substituents most closely resemble those of the present work.[43]

One significant difference between the spectra of $ZC^{+\bullet}$ and $ZCPh^{+\bullet}$ is the loss of the peak hfcc at 1.33 MHz, which strongly suggests that this resonance is due to the proton attached to the 20-position of ZC. This hfcc is somewhat higher than the value of ~0.80 MHz previously measured for pyro-Chl $a^{+\bullet}$;[43] however, part of this difference is attributed to the replacement of Zn for Mg, which is known to cause ~0.20 MHz increases for the α-protons at carbons 10 and 20 for Zn-Chl $a^{+\bullet}$ and Zn-BChl $a^{+\bullet}$, relative to their Mg counterparts. Additionally, the frequency of this $ZC^{+\bullet}$ resonance decreases from 1.48 MHz at 220 K to 1.26 MHz at 170 K, and it is possible that the hfcc measured for $ZC^{+\bullet}$ would be in closer agreement at the 140 K temperature of the previous studies. A second difference between the spectra of $ZC^{+\bullet}$ and $ZCPh^{+\bullet}$ is the reduction of the β-proton hfcc's of carbons 17 and 18, due to substitution of the phenyl group at the 20-position. The nature of this change is discussed below.

(63) Kurreck, H.; Kirste, B.; Lubitz, W. *Electron Nuclear Double Resonance Spectroscopy of Radicals in Solution*; VCH: Weinheim, 1988.

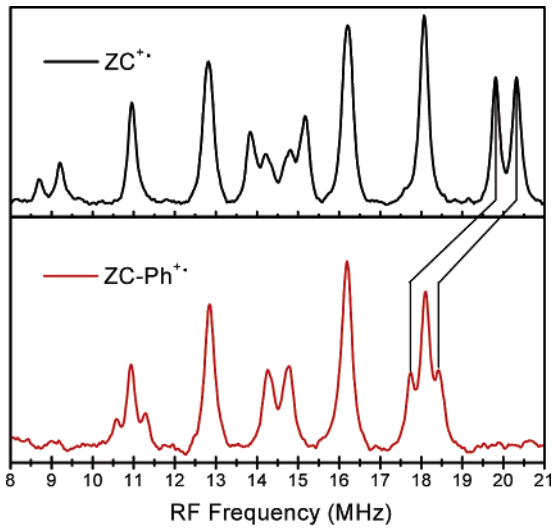

Figure 9. ^{1}H ENDOR spectra of $ZC^{+\bullet}$ (black) and $ZCPh^{+\bullet}$ (red), 0.5 mM in CH_2Cl_2/THF (9:1 v:v) at 195 K. Experimental conditions: frequency modulation, 25 kHz; modulation depth, 100 kHz; time constant, 5.12 ms; scan time, 244 × 21 s; microwave power, 31 mW; RF power, 180−700 W.

Table 4. Proton hfcc's for Chlorin Cation Radicals in DCM/THF (9:1)[a]

		proton assignment				
compd[b,c]	var. β, γ	20	2a, 7a, 8a, 5, 10	12a	18	17
$ZC^{+\bullet}$	0.6	1.33	3.38	7.11	10.61	11.62
$ZCPh^{+\bullet}$	0.5		3.34	7.17	6.46	7.84
Zn-Chl $a^{+\bullet}$	1.02	1.02	3.29, 3.87	7.3	10.8	10.8
pyro-Chl $a^{+\bullet}$		0.80	2.98	6.83	9.93	9.93

[a] Values in MHz. [b] Data for $ZC^{+\bullet}$ and $ZCPh^{+\bullet}$ obtained at 195 K. [c] Data for Zn-Chl $a^{+\bullet}$ and pyro-Chl $a^{+\bullet}$ taken from Table 2 of ref 38, obtained at $T = 140$ K.

Discussion

The data presented in Table 3 show that the rates of electron transfer though a phenyl group attached to the 20-position of a chlorophyll are very rapid, even at relatively modest values of ΔG_{CS}, and result in quantitative charge separation. A comparison of the electron-transfer rates for the ZCPh dyads with those of the corresponding Z3PnPh dyads shows that the rates of both charge separation and recombination differ by less than a factor of 2. Electron-transfer rate constants depend on several parameters involving both the donor−acceptor molecule and its interaction with the surrounding medium. Semiclassical electron-transfer theory shows that the electron-transfer rate constant, k, depends on the electronic coupling matrix element V for the reaction and the free energy of reaction ΔG:[29−31]

$$k = \frac{2\pi}{\hbar}|V|^2\sqrt{\frac{1}{4\pi\lambda_S k_B T}}\sum_{n=0}^{\infty}\exp(-S)\frac{S^n}{n!}\exp\left[\frac{-(\Delta G + \lambda_S + n\hbar\omega)^2}{4\lambda_S k_B T}\right] \quad (4)$$

where $h\omega$ is the vibrational quantum, assumed to be ~1500 cm^{-1}, $S = \lambda_I/\hbar\omega$, λ_I is the internal reorganization energy of the donor−acceptor molecule, λ_S is the solvent reorganization energy, and the summation n is done over the quantum number of the high-frequency vibrational mode. For a given acceptor, ΔG_{CS} for the Z3PnPh dyad is ~0.2 eV more negative than that for the corresponding ZCPh dyad (Table 3); therefore, eq 4 predicts that the charge separation rate constant, k_{CS}, should be somewhat larger for the porphyrin dyad than for the chlorin dyad, provided that λ_S, λ_I, and V_{CS} for charge separation are comparable.

An assessment of the solvent reorganization energy can be made using the Marcus expression for λ_S based on treating the solvent as a dielectric continuum:[64]

$$\lambda_S = e^2\left(\frac{1}{2r_D} + \frac{1}{2r_A} - \frac{1}{r_{DA}}\right)\left(\frac{1}{\epsilon_0} - \frac{1}{\epsilon_S}\right) \quad (5)$$

where ϵ_S and ϵ_0 are the static and high-frequency dielectric constants of solvent, respectively, r_D and r_A are the ionic radii, and r_{DA} is the donor−acceptor distance. Due to the structural similarities between pairs of ZCPh and Z3PnPh dyads having a given acceptor, the ionic radii and the donor−acceptor distances are essentially identical (see Supporting Information). For toluene, $\epsilon_S = 2.38$ and $\epsilon_0 = 2.25$, so that eq 5 yields $\lambda_S = 0.03$ eV, while for THF, $\epsilon_S = 7.58$ and $\epsilon_0 = 1.98$, so that $\lambda_S = 0.43$ eV.

Evaluating λ_I for photoinduced charge separation reactions is difficult because there is no independent way to assess the degree of electronic interaction between ^{1}*ZCPh and ^{1}*Z3PnPh with a given acceptor. For example, accurate excited-state electronic structure calculations on molecules of this size are not practical. However, photoexcitation of molecules with large π systems frequently results in only small structural changes on going from the ground state to the relaxed excited state. The total reorganization energy, λ, where $\lambda = \lambda_S + \lambda_I$, for formation of the relaxed ^{1}*ZCPh and ^{1}*Z3PnPh states from their corresponding ground states can be estimated from the Stokes shifts between their optical absorption and emission spectra, where $\lambda = (E_{abs} - E_{em})/2$. Using the data in Table 1, $\lambda \leq 0.02$ eV for the formation of both ^{1}*ZCPh and ^{1}*Z3PnPh, so that the structural changes that occur upon formation of these excited states are neglible. This means that λ_I for both charge separation and recombination can be calculated by considering only geometry changes between the ground state and the radical-ion-pair state. For a given acceptor, its contribution to λ_I for both charge separation and recombination is the same within each pair of chlorin and porphyrin dyads, so that the entire difference in λ_I is due solely to the differences between λ_I for the chlorin and porphyrin radical cations. For each radical cation, λ_I was calculated using eq 6:

$$\lambda_I = E_0^+ - E_0 \quad (6)$$

where E_0^+ is the energy of the ground state at the radical cation geometry and E_0 is the energy of the ground state in its energy-minimized conformation. These energies were calculated by unrestricted DFT using the PW91 functional and the 6-31G* basis set,[55] to give $\lambda_I = 0.14$ eV for $ZCPh^{+\bullet}$/ZCPh and $\lambda_I = 0.10$ for $Z3PnPh^{+\bullet}$/Z3PnPh (see Supporting Information). The similarity of the internal reorganization energies is reasonable, given that the positive charge within each radical cation is delocalized over a relatively large π system. These calculations show that λ_I does not change significantly between the chlorin and the porphyrin.

Given that λ_S and λ_I are essentially the same for both charge separation and recombination for the ZCPh and Z3PnPh dyads with a given acceptor in a particular solvent, the differences observed for the charge separation and recombination rates must be due to differences in ΔG and/or V. Unfortunately, there is no independent way to estimate the differences in V between the chlorin and porphyrin series. Nevertheless, using the measured values of k and ΔG along with the values of λ_S and λ_I given above, eq 4 can be used to estimate V. The data presented in Table 3 show that all the values of V_{CS} and V_{CR}, comparing the ZCPh and Z3PnPh dyads with a given acceptor in a particular solvent, are within a factor of 2 of each other, suggesting that electronic coupling for photoinduced charge separation and recombination through the 20-position of the chlorin is similar to that of the porphyrin.

The Z3PnPh porphyrin was chosen specifically as a reference molecule because its one-electron oxidation potential differs by only 0.01 V from that of ZCPh, so that the ΔG_{CR} values for the charge recombination reactions for ZCPh and Z3PnPh dyads having a given acceptor in a particular solvent are very similar. This similarity assumes that the entire radical-ion-pair population recombines directly to the singlet ground state and is not complicated by radical pair intersystem crossing,[65−68] in which a substantial fraction of the population could recombine to give ^{3}*Z3PnPh or ^{3}*ZC. Since the energies of ^{3}*Z3PnPh and ^{3}*ZC are ~1.7 and ~1.3 eV, respectively, charge recombination to these triplet states would have very different values of ΔG_{CR}. This fact, combined with the presence of two parallel charge recombinations pathways, would make further comparisons of V_{CR} between the chlorin and porphyrin series for these reactions difficult. The data in Table 3 show that the radical-ion-pair energies of the ZCPh dyads in toluene are all slightly above that of ^{3}*ZC, while those of the Z3PnPh dyad are slightly below. In THF, all of the radical-ion-pair energies are below those of the triplet states of the macrocyclic donors. This suggests that charge recombination rates from a triplet radical ion pair to the neutral triplet states should be quite slow and noncompetitive with charge recombination to the singlet ground state. The transient absorption data in Figures 6−8 and Figures S6−S8, S11−S16 confirm that charge recombination in all the dyads presented here does not produce any significant yield of long-lived triplet products.

Another potential source of variability in the calculated values of V due to small differences in ΔG may arise specifically in low-polarity solvents, such as toluene. Whenever λ_S is very small, as is the case for toluene, rate constants calculated using eq 4 show oscillations with a period of $\hbar\omega$ near the top of the rate vs free energy profile as well as in the inverted region. For small variations in the magnitude of ΔG, these oscillations can

(64) Marcus, R. A. *J. Chem. Phys.* **1965**, *43*, 679−701.
(65) Weller, A.; Staerk, H.; Treichel, R. *Faraday Discuss., Chem. Soc.* **1984**, *78*, 271−278.
(66) Hoff, A. J.; Gast, P.; van der Vos, R.; Franken, E. M.; Lous, E. J. *Z. Phys. Chem.* **1993**, *180*, 175−192.
(67) Steiner, U. E.; Ulrich, T. *Chem. Rev.* **1989**, *89*, 51−147.
(68) Till, U.; Hore, P. J. *Mol. Phys.* **1997**, *90*, 289−296.

result in significant differences in the calculated value of V. When λ_S is large, as is the case for THF, there are no oscillations in the rate vs free energy profile, so that small variations in ΔG will not affect V. To determine whether this issue affects the results for the molecules examined here, we obtained a complete set of charge separation and recombination time constants in THF (Table 3). Comparing the data for the ZCPh and Z3PnPh dyads with a given acceptor in THF, both V_{CS} and V_{CR} do not vary by more than a factor of 2, similar to the results in toluene, so that the observed differences of V_{CS} and V_{CR} between the chlorins and porphyrins in toluene are most likely not due to oscillatory behavior in the rate vs free energy profile.

The value of V_{CR} can be related to several parameters associated with the molecular orbitals on the donor and acceptor by the approximate expression[32]

$$V_{CR} = K \sum_i \sum_j c_i^{D} c_j^{A} S_{ij}^{DA} \quad (7)$$

where c_i^D and c_j^A are the atomic orbital coefficients of the relevant MOs on the donor atoms i and acceptor atoms j, S_{ij}^{DA} is the overlap integral of atomic orbitals on D and A, and K is an empirical constant. As discussed above, the Z3PnPh HOMO has a_{2u} symmetry,[37] while the ZCPh HOMO should have a_2 symmetry, which has a charge distribution similar to that of the metalloporphyrin a_{1u} orbital. This should place much more charge density at the 20-position of $ZnPnPh^{+\bullet}$ than on that of $ZCPh^{+\bullet}$, resulting in a much larger value of V_{CR} (eq 7) and consequently a much faster rate of charge recombination for the porphyrin-containing radical ion pairs. Since this is contrary to what is observed, we used ENDOR spectroscopy to establish the electron density distribution within $ZCPh^{+\bullet}$.

ENDOR spectroscopy of Chl $a^{+\bullet}$ in solution shows that the hfcc's of the peripheral alkyl groups on Chl $a^{+\bullet}$ are large, while the splittings of the protons at the meso positions (5, 10, and 20) are very small.[43] This is consistent with the HOMO of Chl $a^{+\bullet}$ having a_2 symmetry. Very similar electron density distributions are observed for both $ZC^{+\bullet}$ and $ZCPh^{+\bullet}$. The only significant difference between the hfcc's observed for $ZC^{+\bullet}$ and $ZCPh^{+\bullet}$ involves the protons at the 17 and 18 carbon atoms. The hfcc's for the remaining protons do not change significantly. The β-proton hfcc's (in MHz) are related to the dihedral angle between the π-orbital bearing the spin density and C−H bond by eq 8:[38,69,70]

$$a_H = \rho_c(-9.2 + 96.7 \cos^2 \theta) \quad (8)$$

where ρ_c is the spin density on the α-carbon of the π-system and θ is the dihedral angle between the axis of the p_z orbital of the α-carbon in the π-system and the $C_\beta-H_\beta$ bond. Unrestricted DFT spin density calculations (Table S3) show that ρ_C for the 16- and 19-positions of $ZC^{+\bullet}$, which are the relevant α-carbons, are both reduced upon incorporation of the 20-phenyl group in $ZCPh^{+\bullet}$. Using eq 8 and the data in Tables 4 and S3, and assuming that the calculated values of ρ_C are dominated by the π spin density at the α-carbon, the calculated dihedral angles, θ, for the 17 and 18 β-protons in $ZCPh^{+\bullet}$ are 28° and 30°, respectively, while those for $ZCPh^{+\bullet}$ are 31° and 42°, respectively. The reduction in the hfcc's is consistent with a small distortion of the geometry in ring D around the 17- and 18-positions due to steric hindrance of the 20-phenyl group.

As noted previously,[43] the effect of substitution does not cause the long-range changes that would be expected if the molecular orbital occupation were different for $ZC^{+\bullet}$ and $ZCPh^{+\bullet}$. The ENDOR data allow us to conclude that the addition of the 20-phenyl does not change the electronic structure of the zinc chlorin radical cation significantly, which is completely consistent with the HOMO having approximate a_2 symmetry. The hfcc's observed using ENDOR are also consistent with the spin (and charge densities) calculated using DFT (Table S3), which show that $\rho_C = 0.03$ for the 20-positions of both $ZC^{+\bullet}$ and $ZCPh^{+\bullet}$. These results leave us with a significant discrepancy. The charge distributions within $ZCPh^{+\bullet}$ and $Z3PnPh^{+\bullet}$ are both consistent with established patterns present in related macrocycles, which leads us to expect that V_{CR} and k_{CR} for the Z3PnPh dyads should be significantly larger than that for the corresponding ZCPh dyads. This, however, is not observed. To examine this point further, we used DFT calculations to compare the electronic structures of $ZCPh^{+\bullet}$ and $Z3PnPh^{+\bullet}$.

DFT calculations (PW-91, 6-31G*) were used to obtain the charge (and spin) density distributions of the HOMOs of $ZCPh^{+\bullet}$ and $Z3PnPh^{+\bullet}$ (Figure 10A,B). The $Z3PnPh^{+\bullet}$ HOMO has an electron density distribution typical of a porphyrin a_{2u} orbital, which is consistent with previous DFT calculations and with well-established experimental evidence in the porphyrin field.[71,72] In contrast, the electron density distribution within the HOMO of $ZCPh^{+\bullet}$ indicates that the HOMO has a_2 symmetry, which appears as a mixture of the distributions characteristic of metalloporphyrin a_{1u} and a_{2u} orbitals. This phenomenon has been observed previously for water-ligated chlorophyll molecules and is attributed to a Jahn−Teller distortion of the macrocycle resulting from ligation of the metal center.[40,73,74]

A contributing factor to the similarity of the values of V_{CR} for the ZCPh and Z3PnPh dyads might be a discrepancy between the dihedral angles that the π-system of the 20-phenyl group makes with the π-systems of $ZCPh^{+\bullet}$ and $Z3PnPh^{+\bullet}$. If this dihedral angle is defined as 0° when the two π-systems are coplanar, the DFT calculations show that the dihedral angles for $ZCPh^{+\bullet}$ and $Z3PnPh^{+\bullet}$ are 75° and 60°, respectively. This suggests that $\pi-\pi$ overlap of the phenyl group with the macrocycle is slightly larger for $Z3PnPh^{+\bullet}$, so for a given acceptor, the calculations predict that V_{CR} for $Z3PnPh^{+\bullet}$ should be larger than that for $ZCPh^{+\bullet}$. Thus, the calculated differences in the dihedral angle of the 20-phenyl group do not account for the similar values of V_{CR} observed for the $ZCPh^{+\bullet}$ and $Z3PnPh^{+\bullet}$ dyads.

In essentially all previous considerations of the influence of electronic coupling on rates of both energy and electron transfer to or from porphyrins and chlorophylls, the analysis of rate changes as a function of electronic structure focuses on the electron density distribution in the relevant orbitals of the macrocycles. For electron-transfer reactions, the presence of the

(69) Heller, C.; McConnell, H. M. *J. Chem. Phys.* **1960**, *32*, 1535−1539.
(70) Stock, L. M.; Wasielewski, M. R. *J. Am. Chem. Soc.* **1973**, *95*, 2743−2744.
(71) Spellane, P. J.; Gouterman, M.; Antipas, A.; Kin, S.; Liu, Y. C. *Inorg. Chem.* **1980**, *19*, 386-391.
(72) Vangberg, T.; Lie, R.; Ghosh, A. *J. Am. Chem. Soc.* **2002**, *124*, 8122−8130.
(73) Song, H.; Reed, C. A.; Scheidt, W. R. *J. Am. Chem. Soc.* **1989**, *111*, 6868−6870.
(74) Prendergast, K.; Spiro, T. G. *J. Phys. Chem.* **1991**, *95*, 9728−9736.

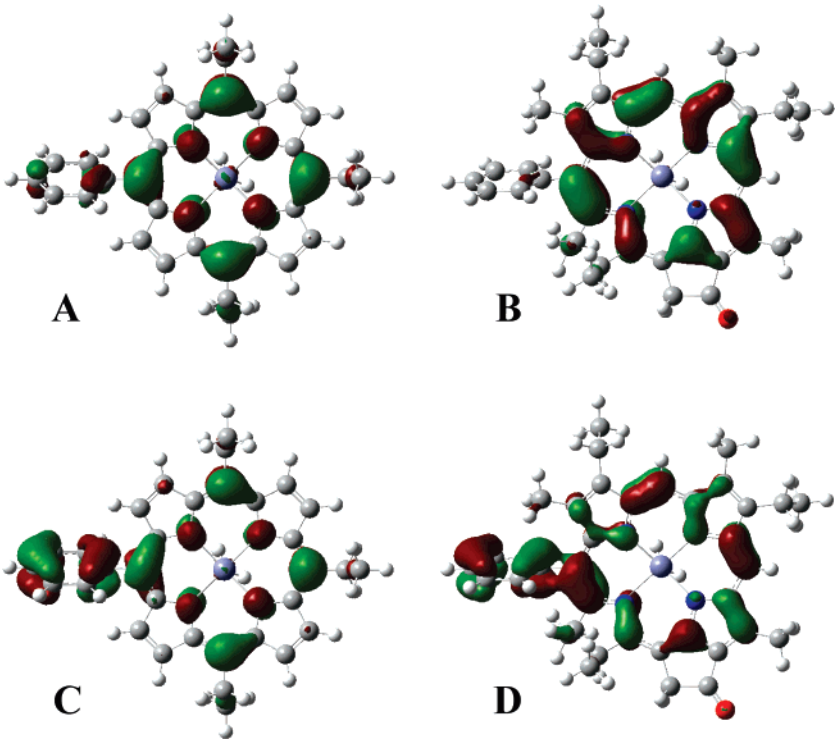

Figure 10. HOMOs of model compounds for Z3PnPh$^{+\bullet}$ (A) and ZCPh$^{+\bullet}$ (B). The perturbation caused by the presence of negative partial point charges are shown in (C, D) (see text).

partner donor or acceptor is often neglected. For cases involving energy transfer, where the donor and acceptor are both neutral molecules, this assumption generally causes few difficulties. However, photoinduced electron transfer within covalently linked donor−acceptor molecules often places the photooxidized donor at a highly restricted distance and orientation relative to the reduced acceptor. Under these circumstances, the charge distributions of each partner ion can have a significant influence on the overall charge distribution within the radical ion pair. At the simplest level, this distortion is due to Coulombic attraction of the positive and negative charges. Measurements of charge distributions within the chemically oxidized chlorin or porphyrin donors using EPR or ENDOR measurements of their spin distributions do not capture these distortions. The counterions that are present following chemical or electrochemical generation of the chlorin and porphyrin radical cations do not occupy a single unique position relative to the macrocycle, so their electrostatic influence on the charge distributions of the radical cations is averaged out in solution.

Previous DFT calculations performed on NI$^{-\bullet}$ and PDI$^{-\bullet}$ reveal that the majority of the negative charge density resides on the carboximide oxygen atoms.[75] While it is not yet possible to model the overall radical-ion-pair charge distribution using current computational methods, we have modeled the influence of the negative charge density due to the radical anion on the electronic structure of both ZCPh$^{+\bullet}$ and Z3PnPh$^{+\bullet}$. DFT calculations were performed on these radical cations with two −0.5 charges located where the nearest carbonyl oxygen atoms of the acceptor would reside in the complete donor−acceptor dyad. Although the aforementioned DFT calculations on PDI$^{-\bullet}$ alone place only ∼25% of the negative charge density on each oxygen atom, we assume that Coulombic interactions between the radical pairs result in a larger portion of the negative charge density residing on the dicarboximide closest to the electron donor. The calculations with the two fixed −0.5 charges reveal that the presence of the negative charges significantly shifts the charge density of both radical cations from the macrocyclic core onto their bridging phenyl rings (Figure 10C,D). As a result, the atomic orbital coefficients on the donor atoms i, c_i^{D},[76,77] relevant to the electronic coupling matrix element, V_{CR} (eq 7), are actually quite similar for the different donor chromophores (see Table S4). This effect should be more pronounced in low-polarity solvents, e.g. toluene used in this study, than it would be in highly polar solvents in which the charges are more effectively screened from one another by the high dielectric constant of the medium. Therefore, the presence of an adjacent covalently linked radical anion at a fixed location relative to the radical cation significantly alters the electron densities on both ZCPh and Z3PnPh, which results in nearly identical values of V_{CR}, and consequently k_{CR} for charge recombination. We are currently performing a more extensive DFT computational study on macrocyclic radical cations in the presence of charge distributions characteristic of adjacent acceptors at fixed distances and orientations relative to the macrocycle to better simulate the charge distributions of the donor−acceptor pairs and V_{CR}.

Conclusions

Suzuki cross-coupling reactions have afforded 20-phenyl-substituted Chl *a* derivatives in good yields and significant quantities from readily available Chl *a*. The versatility of this

(75) Weiss, E. A.; Wasielewski, M. R.; Ratner, M. A. *J. Chem. Phys.* **2005**, *123*, 064504/064501−064504/064508.

(76) Gorelsky, S. I. *AOmix: Program for Molecular Orbital Analysis*; York University: Toronto, Canada (http://www.sg-chem.net), 1997.

(77) Gorelsky, S. I.; Lever, A. B. P. *J. Organomet. Chem.* **2001**, *635*, 187−196.

new functionality has resulted in the synthesis and characterization of a series of ZCPh−arylene bis(dicarboximide) donor−acceptor dyads. In addition to synthetic flexibility, arylation of the 20-position preserves the 13^2 keto and 17^3 ester groups that direct its self-association, while keeping the electron acceptor at a position that should not interfere with known chlorophyll aggregation motifs. Comparing these molecules to an analogous zinc 5,10,15-tri(*n*-pentyl)-20-phenylporphyrin−acceptor (Z3PnPh−acceptor) series shows that the rates of photoinduced charge separation and recombination differ by less than a factor of 2. However, EPR and ENDOR spectroscopy corroborated by DFT calculations show that the highest occupied MO of $ZCPh^{+\bullet}$ has little spin (charge) density at the 20-carbon atom, whereas $Z3PnPh^{+\bullet}$ has significant spin (charge) density. DFT calculations on $ZCPh^{+\bullet}$ and $Z3PnPh^{+\bullet}$ with two −0.5 charges located where the nearest carbonyl oxygen atoms would reside in the complete donor−acceptor dyad show that the presence of the negative charges significantly shifts the charge density of both $ZCPh^{+\bullet}$ and $Z3PnPh^{+\bullet}$ from the macrocycle onto the phenyl rings. These results suggest that the use of measured and/or calculated charge distributions in free radical ions to estimate electronic coupling matrix elements for electron transfer most likely gives erroneous results when covalently linked radical ions are positioned across a short spacer at a fixed distance from one another.

Acknowledgment. The authors thank Mr. J. A. Vura-Weis and Dr. B. Rybtchinski for many valuable discussions, along with Drs. M. J. Ahrens and S. E. Miller for synthetic and spectroscopic assistance. M.J.T. acknowledges the donors of the American Chemical Society Petroleum Research Fund for partial support of this research. This research was supported by the Division of Materials Sciences, Office of Basic Energy Sciences, U.S. Department of Energy, under Contract No. W-31-109-ENG-38. The Bruker E580 spectrometer was purchased with partial support from NSF Grant No. CHE-0131048. The authors also thank BASF AG for a generous gift of bis-(pinacolato)diboron.

Supporting Information Available: Details regarding the synthesis and characterization of the molecules used in this study; the $\Delta G/\lambda_i$ calculations; additional transient absorption data, including Figures S1−S20 and Tables S1−S4; and the complete list of authors for ref 54. This material is available free of charge via the Internet at http://pubs.acs.org.

JA058233J